PNAS
www.pnas.org

Supplementary Information for

Cochlear partition anatomy and motion in humans differ from the classic view of mammals

Stefan Raufer, John J. Guinan Jr., and Hideko Heidi Nakajima

Stefan Raufer
E-mail: sraufer2@gmail.com

This PDF file includes:

Supplementary text
Figs. S1 to S4
References for SI reference citations

Supporting Information Text

Cochlear partition anatomy of humans and various laboratory-animal species

To provide perspective on the anatomy of humans versus laboratory animals, we present the cochlear anatomy of five species and of humans. The anatomy and motion in the base of these laboratory animals served as the main source for the generalized classic view of mammalian cochlear mechanics. The cross-sectional anatomy is shown for the basal part of the cochleas in Fig. S1 and for the apical part in Fig. S2. In each of the five laboratory species, cochleas of at least three different animals were studied, and because the images within a species were all similar, a representative image of each species and location is shown.

There are two major differences between the basal cochlear partition (CP) anatomy of humans and the classic view from laboratory animals: the presence of soft tissue between the osseous spiral lamina (OSL) and basilar membrane (BM) (i.e. a "bridge" region), and the positioning of the TM-limbus attachment above soft tissue as opposed to above OSL bone. Although we have found a bridge-like region in the apex of some animals (see Fig. S2), an unresolved question is how similar these regions are to the human bridge, i.e. do these regions have the same anatomical characteristics as the bridge in humans, such as radial collagen fibers (1). The second difference, the position of the TM-limbus attachment, is important because this position has implications for whether the medial end of the TM moves, or whether it is stationary as is assumed in classic cochlear models. If the TM-limbus attachment is over a bridge-like region with no bone, then it is much more likely that the TM attachment point moves in response to sound than if the TM-limbus attachment is over the bony OSL. The images in Figs. S1 and S2 shed light on these questions, but much more detailed anatomical and physiological work is needed to fully answer them.

The images in Figs. S1 and S2 are of histologically prepared sections stained with Hematoxylin and Eosin from the Otopathology Laboratory at our institution. To estimate the locations along the cochlea, we measured the BM widths from the sections shown in the figures, and translated BM width to cochlear location using published data: for human (2), guinea pig (3), mouse (4), gerbil (5), cat (6), and chinchilla (7). Greenwood maps of these species were used to translate cochlear location to best-frequency (BF) (8).

The basal-turn locations in Fig. S1 are approximately one-quarter to one-half cochlear turn from the basal end of the cochlea (distance from base labeled above each panel). Some general observations from Fig. S1 are: (i) the OSL bone comes close to or overlaps with the inner pillar of the organ of Corti (OoC) in all species but human (the lateral extent of OSL indicated by upward pointing arrows); (ii) the TM-limbus attachment (downward pointing arrows) is above the bridge in humans but above the bone of the OSL in all other species.

The cochlear anatomies of the apical-turn are shown in Fig. S2. They are 80–90% of the total cochlea length from the base. Some observations from Fig. S2 are: (i) the apical OSL appears shorter compared to the basal OSL in Figure S1 (varying across species); (ii) the lateral edge of the OSL bone (upward pointing arrows) overlaps with the inner pillar of the OoC only in gerbil. In the other species, a soft-tissue region, similar to a bridge, exists between the OSL and BM (the guinea pig shows virtually no OSL bone in the apex, which was also noted by Fernandez (3)); (iii) the TM-limbus attachment (downward pointing arrows) is over the bridge in humans and guinea pigs, but over the OSL bone in other species.

The observation of a CP bridge-like region in the apex of guinea pigs led us to reexamine motion measurements in the guinea pig apex to look for possible motion consequences of the soft-tissue region. Warren et al. (9) presented motion measurements said to be from across the width of the BM in the guinea pig apex. In their figure 3E, they show "BM" motion measurements over a radial distance of $\sim$300 μm (if the exponential fit to their data is extrapolated, "BM" motion would be over a $\sim$400 μm range). However, the guinea pig BM shown in their figure 4B has a width of only $\sim$200 μm. One explanation of these results is that Warren et al. measured motion over both the BM and a mobile CP bridge, but they attributed all of the measurements to the BM because they thought that only the BM had significant transverse motion. If so, the data of Warren et al. would be evidence for motion in a CP bridge region in a live animal. These measurements of cochlear motion, and many others, have not coordinated the motion measurements with the corresponding anatomy.

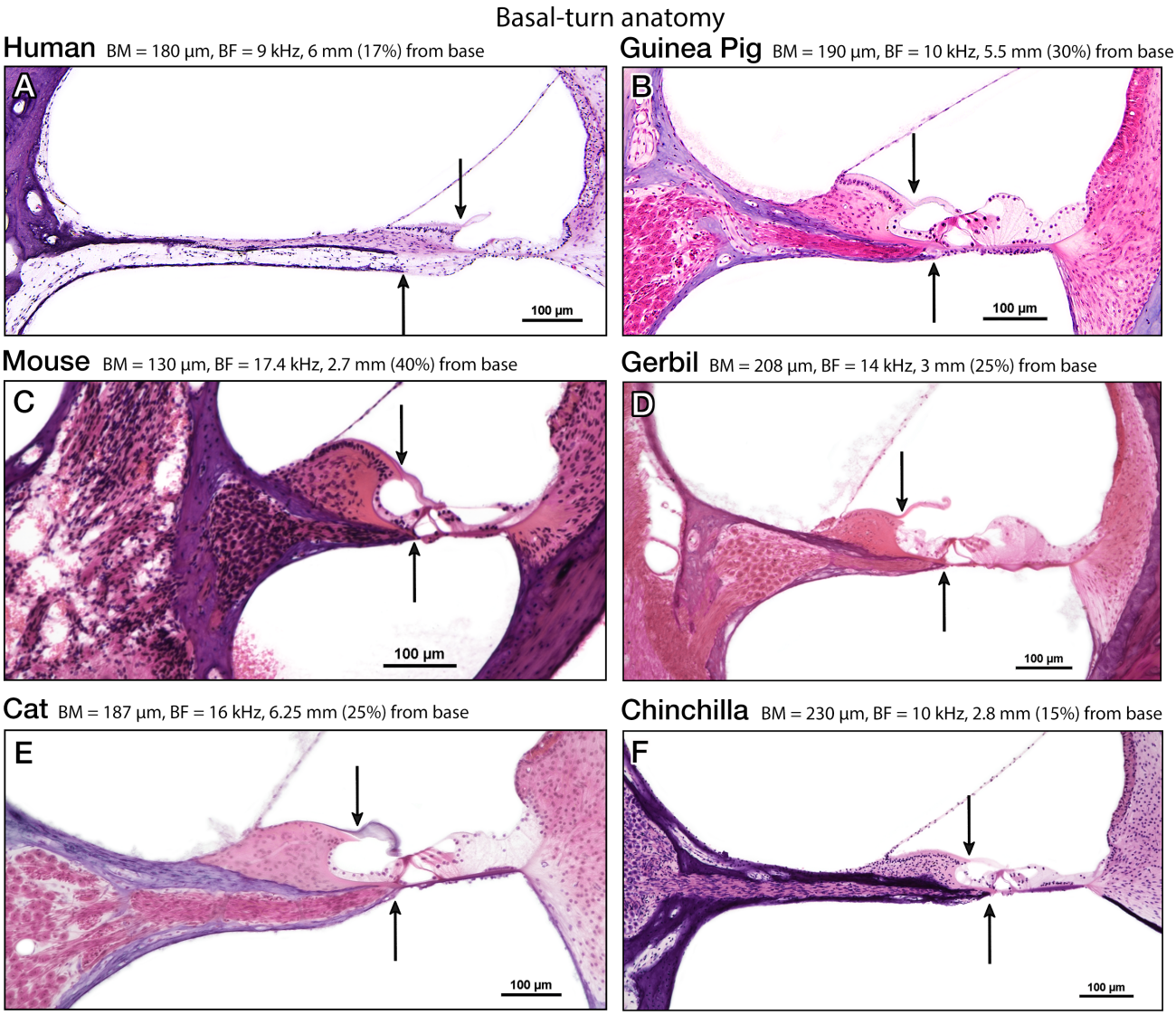

Fig. S1. Basal-turn cross-sectional cochlear anatomy of six species used in cochlear mechanical measurements: (A) Human, (B) guinea pig, (C) mouse, (D) gerbil, (E) cat, and (F) chinchilla. These sections are near the regions where many CP motion measurements have been made. In each, an up-arrow points up to the most lateral extent of bone of the osseous spiral lamina (OSL), and a down-arrow points to the attachment of tectorial membrane (TM) to the limbus. In all species but human, the bone of the OSL extends near to, or underneath, the inner pillar cells of the organ of Corti. In all species but human, the TM-limbus attachment point sits on top of OSL bone (compare the medial/lateral locations of the down-arrows with the up-arrows). Above each panel: the width of the basilar membrane (BM), the best frequency (BF) of the section, and the distance of the section from the basal end of the cochlea.

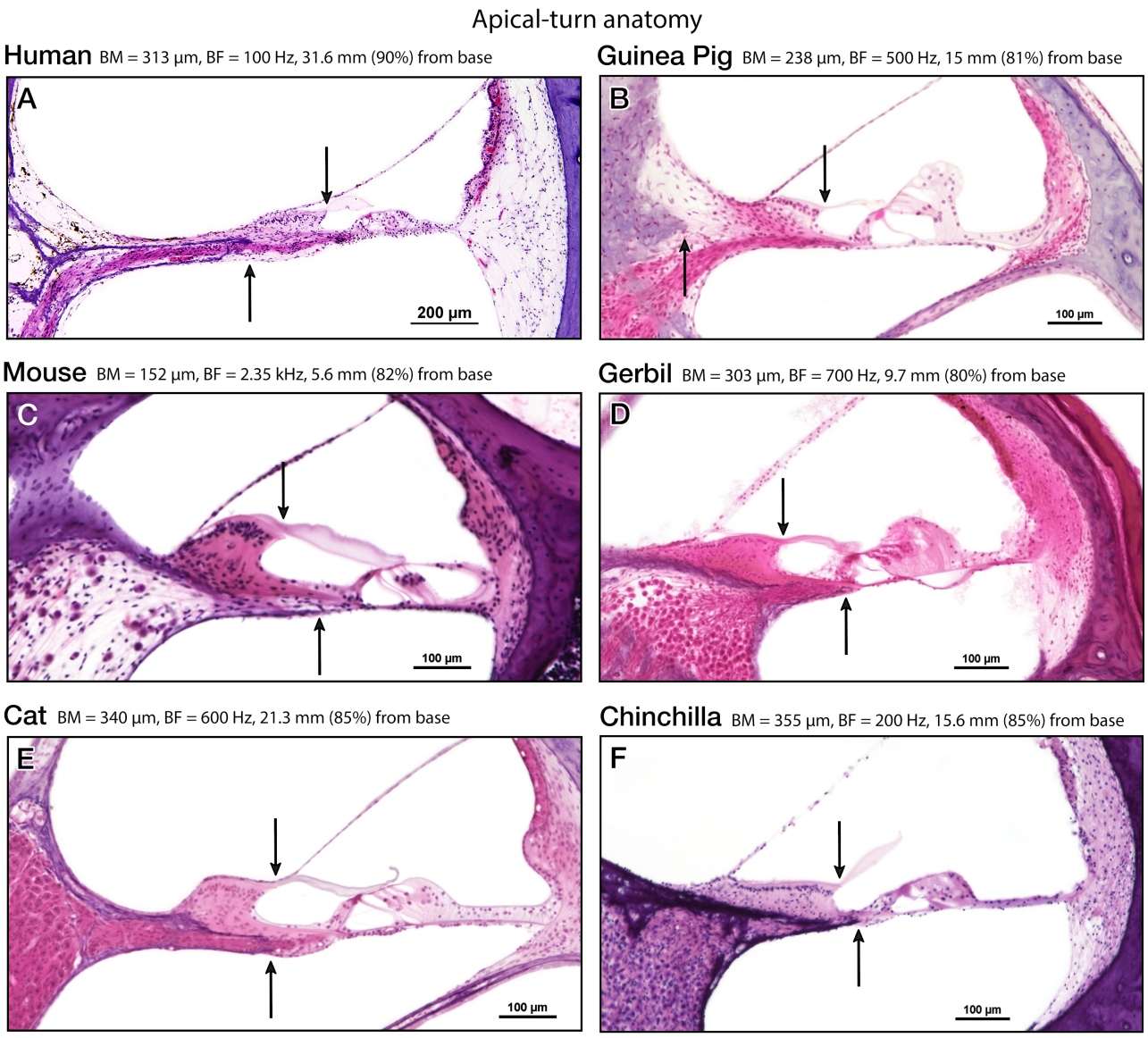

Fig. S2. Apical-turn cross-sectional cochlear anatomy of the six species of Fig. S1. The lateral edge of the OSL bone (upward pointing arrow) extends to underneath the inner pillar cells only in gerbil. A soft-tissue bridge between the OSL and BM is seen in all species except gerbil. Across species, these soft-tissue regions vary in width with respect to the BM. In chinchilla, the soft-tissue region is short, while in the guinea pig there is virtually no bony OSL in the apical turn. The spiral limbus (including the limbal attachment of the tectorial membrane (TM)) sits on the soft-tissue CP bridge in human and guinea pig, and on the bony OSL in the other species. Above each panel: the width of the basilar membrane (BM), the best frequency (BF) of the section, and the distance of the section from the basal end of the cochlea.

Cochlear partition motion from six human temporal bones

Figure S3 presents radial velocity profiles and tuning curves for all six specimens tested.

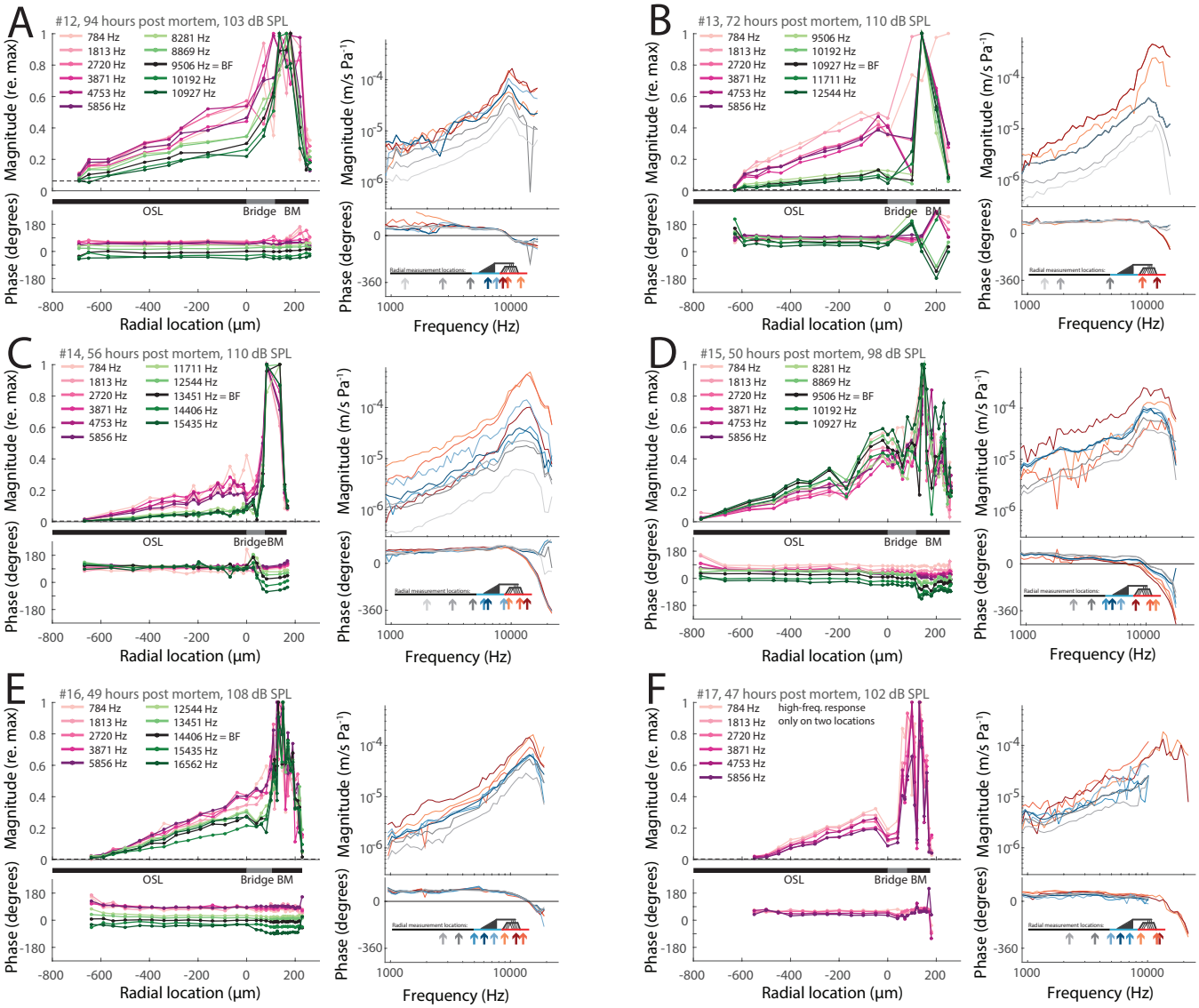

Fig. S3. Radial profiles and tuning curves of cochlear partition (CP) transverse motion from six human temporal bones. (A-F) Each panel is similar to Fig. 2 and is from a location ∼1 mm from the basal end of the cochlea. In panel F, only low-frequency data are shown for velocity versus radial location because high frequency data were only obtained for two BM locations.

Modeling CP movement

In classic cochlear models, CP transverse motion was assumed to be restricted to BM motion, even though there had been evidence for some OSL transverse motion (see main-text Introduction). In classic models the BM was considered fixed at both ends. When systematic measurements of BM transverse motion as a function of radial distance across the BM became available, these provided a basis for modeling BM motion. Guinea-pig BM motion can be accurately modeled with a simple beam representing the BM as shown in Fig. S4A (10, 11). In contrast, the CP of the human involves motion of multiple structures, such as the OSL, bridge, and BM, and is not well represented by a simple beam model. Human CP motions, for below-BF frequencies, can be adequately captured by a composite beam model, as described below.

Methods and Results. A composite beam model was fit to averaged human CP motion data. The model is based on CP measurements for below-BF frequencies, where the whole CP moves in phase. Near and above BF, some BM phase measurements lagged the OSL (Figs. 2, S3) and the beam equations, which apply only to unimodal motion, may not accurately capture the more complex motion at higher frequencies. The data in Fig. S4B (below-BF data from Fig. 3A) were loess-smoothed (locally weighted average (12)), yielding the blue line in Fig. S4B. To account for varying widths across temporal bones, we normalized the x-coordinates of each cross-sectional motion profile by linear scaling of the measurements in each CP region. Scaling was performed so that the BM of each temporal bone was 13.3% of the CP width, the CP bridge was 11.5% of the CP width (83% of the BM) and the OSL was 75.2% of the CP width.

We characterized our measurements of CP motion with a mechanical model of the CP that included a composite beam of two elements: (i) a rigid rod hinged near the modiolus – which emulated the OSL and the medial half of the CP bridge, and (ii) a flexible beam with constant bending stiffness, simply supported at both ends – which emulated the lateral part of the CP bridge and the BM. The rigid rod was hinged with a rotational spring at $x = 0$ (the medial attachment of the OSL) and a hinge near the mid-point of the bridge, which was assumed to have no torsional stiffness (the second derivative with respect to x is continuous). We used similar computations as in Homer et al. (11) (Fig. 5d in Section IV and the Appendix in (11) and adjusted the ratio of the stiffnesses of the two beams (κ in Homer et al.) to best match the averaged data (blue line in Fig. S4B). Our parameters, defined in Homer et al., are: $x_t = 0.81$; $x_1 = 0 : 0.01 : x_t$; $x_2 = x_t : 0.01 : 1$; $\kappa = 10^{-4.95}$; $q = 1$; $EI = 1$. The resulting composite beam model in Fig. S4B shows the overall properties of our CP motion measurements, including the OSL moving as a stiff plate hinged at the modiolus, and the maximum CP motion occurring near the BM-bridge connection (Fig. S4B).

Discussion. Several features of the model are worthy of comment: First, it may seem surprising that the OSL moved as if hinged near its connection with the modiolus. This might be because the OSL bone is porous in that region (13–17), which makes it more flexible and allows a discrete pivot point. Second, a hinge in the middle of the bridge was not expected. A comparison of the model hinge location to anatomical measurements indicates that the hinge is near the lateral end of the limbus and the medial edge of the inner sulcus. The medial region of the bridge parallels the tissue of the limbus, whereas the lateral region of the bridge parallels the inner sulcus and corresponds to an area of low tissue density, and presumably, less torsional stiffness.

Two other modeling studies are relevant. First, Kapuria et al. (18) published a cross-sectional model of the gerbil BM. The gerbil has a very particular BM anatomy with a flexible BM arcuate zone and a stiff BM pectinate zone. Thus, the gerbil has both stiff and flexible parts of the CP, just as are present in humans (although at different structures and locations). The gerbil modeling results suggest that the BF is set mainly by the properties of the more flexible part of the CP (in humans, the BM) with relatively little influence from the stiff part (in humans, the OSL). If this concept from the gerbil is translated to our findings, the relatively large volume displacement of the OSL may play only a minor role in setting the BF of the human cochlea. Second, a cross-sectional model by Taber and Steele (19) included three CP regions, namely the OSL, BM arcuate zone (stiffened by the arches of Corti), and the BM pectinate zone. This model compared the BM motion with a very stiff OSL (typical of most mammals) to the BM motion with a flexible OSL (said to be typical of primates) and found that the model with the flexible OSL produced longer phase delays, as observed in squirrel monkey BM recordings (20). In Kapuria et al.'s and Taber and Steele's models, even though the volume displacement of the near-rigid OSL (or near-rigid BM region) was large compared to the flexible BM region, the properties of the near-rigid region had relatively little effect on the traveling wave other than its phase and did not substantially change the BF.

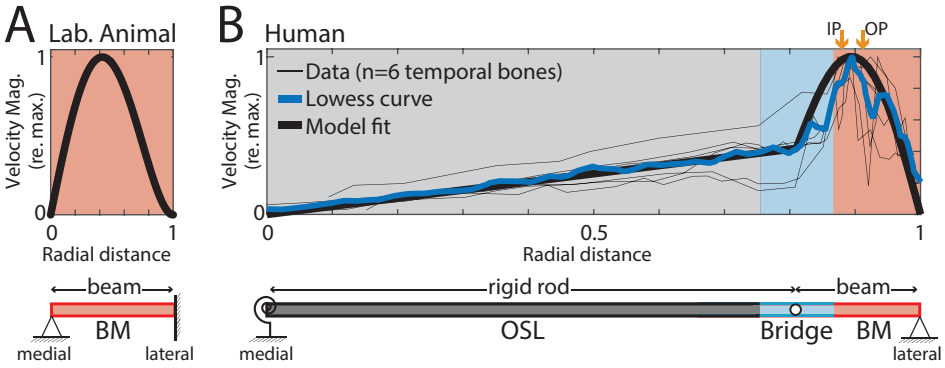

Fig. S4. Plots of model fits to cochlear partition (CP) motion in laboratory animals (A) and humans (B), each normalized by its peak value. (A) In a laboratory animal (guinea pig), basilar membrane (BM) motion was approximated by a mechanical beam model in which the BM was simply supported at the osseous spiral lamina (OSL) ($x = 0$) and clamped at the spiral ligament ($x = 1$) (from Homer et al. (11)). (B) In humans, CP motion was fit by a composite beam model consisting of a rigid rod hinged to a flexible beam. The thin black lines plot the average of below BF measurements (as in Fig. 3A) for each human specimen. The blue line is a loess curve (a locally weighted averaging) of the measurements from all six ears. The thick, black line represents the motion of the composite beam model. Orange arrows point to estimated locations of the bottoms of the inner pillar (IP) and outer pillar (OP).

Methods

Temporal bones. We used seventeen unidentified fresh human cadaveric temporal bone specimens from the consented donor program at Massachusetts General Hospital. The first eleven specimens were used to perfect the technique. We report here results from six ears, 53 to 78 years old (mean = 60.2 years). All were left ears (to keep the measuring set-up consistent) and four were male. Details regarding the removal and initial preparation of the temporal bones, as well as our criteria to assess the condition of the bones are described in Nakajima et al. (21) and Frear et al. (22). Immediately after extraction, specimens were kept in 0.9% saline and refrigerated at 0-4 degrees Celsius. After drilling and preparing a fresh (never frozen) specimen for measurement, we made reference measurements of stapes velocity, RW membrane velocity, and intracochlear pressures. Experiments were performed at room temperature, 47 to 108 hours post mortem. Post mortem times are defined as the time from death to the beginning of CP motion measurements.

To prepare for CP motion measurements, we removed the semi-opaque round window (RW) membrane with the sharp edge of a hypodermic needle to provide an unobstructed view of the cochlear partition. To prevent fluid leakage from the cochlea, and air entering through the open RW, the temporal bone was oriented with the CP at the RW region in a horizontal plane facing upward. The fluid level was controlled with absorbent tips (#503, Henry Schein) so that over the CP there was only a thin fluid film to avoid possible measurement artifact due to motion of the fluid-air boundary that differed from the motion of the CP (23). The removal of fluid in scala tympani reduced the mass seen by the CP. However, at low frequencies where the effect of mass is negligible, CP motion would not be affected by this reduction in mass. At high frequencies (>5-10 kHz) the fluid loading may change the response of the CP.

Sound stimulation. Acoustic pure tones between 100 Hz and 24 kHz (10 per octave) were generated by a Radio Shack driver (400-1377) and delivered to the ear canal with a flexible polyethylene tube. The sound pressure level in the ear canal 1 mm from the tympanic membrane was monitored with a calibrated probe-tube microphone (Knowles EK-23103-000, calibrated against a Larsen Davis 2541), which was fed through a metal sleeve that penetrated the bony ear canal. Sound pressure level was kept constant as a function of frequency in each bone (iso-input), but was varied across experiments (from 94–110 dB SPL) to produce adequate signal strengths for the laser Doppler vibrometer.

Laser Doppler velocity measurements. A laser Doppler vibrometer (LDV) (Polytec CLV 700) was used to measure the velocities of the posterior crus or footplate of the stapes, the center of the RW membrane, and along the scala tympani surface of the CP. Reflective polystyrene microbeads (50 μm diameter, $\sim$0.07 μg each) were used to enhance the signal-to-noise ratio for stapes and RW measurements. For CP measurements, the laser beam was oriented perpendicular to and focused on the scala-tympani surface of the CP. This provided adequate reflections without microbeads (e.g. as in (24)). The radial position of the CP measurement point was controlled with a micromanipulator. We measured up to 34 radial locations on the CP using 5 μm radial-position steps on the BM and bridge, and 50 μm steps on the OSL, skipping points where the reflectivity was too low. Thus, we depended on CP reflectivity, resulting in varied measurement locations across specimens. In our system the laser-beam spot size on the tissue can be as large as 37 μm (as indicated by Polytec specifications), but the actual spot size was visually smaller, and 5 μm movements often produced large changes in reflectivity. Thus, we think that the spot size did not produce substantial spatial smoothing in our data. The depth of field of the laser Doppler measurements (according to Polytec specification) is theoretically 2 mm, however, in this passive preparation the deeper structures are expected to vibrate the same as the surface CP. In several early experiments, we measured the motion of reflective microbeads (5–20 μm diameter) on the CP surface, washed them away, measured at the same spot and found similar velocities, i.e. motions within 2 dB and phases within 15 degrees, with similar CP velocity measurements with and without beads.

In five temporal bones we obtained data up to one-half octave above the BF. In one temporal bone, low laser signals prevented obtaining reliable near-BF data. For temporal bone #16 (used for Fig. 2), we excluded the CP motion at f=4700 Hz because an anti-resonance in stapes velocity decreased the sound pressure in scala vestibuli by 40 dB. In one temporal bone (#15), during removal of the RW membrane, the OSL was punctured 1 mm apical to the measurement location. This caused stapes velocity and intracochlear sound pressure to change in a small frequency band centered around 2 kHz by less than 5 dB, but the measurements were unchanged for frequencies below 1.5 kHz and above 3 kHz, thus these data were used in Fig. 3 and S4. To determine possible vibrational coupling of the ear-canal sound to the temporal bone, we measured the velocity of the cochlear promontory during acoustic stimulation; all CP motion presented was $\sim$10–20 dB larger than cochlear promontory motion.

Intracochlear pressure measurements. Fiber-optic pressure sensors developed by Olson (25) were used to record sound pressure in the vestibule (21, 26). Details regarding the calibration and placement of a sensor in the vestibule are given elsewhere (21, 22, 27). Initial intracochlear pressure was measured with the RW membrane intact and then again after the RW was removed. Removing the RW caused minimal changes (<3 dB) in intracochlear pressures for all tested frequencies.

Anatomical measurements. During an experiment, when the human CP is viewed through an operating microscope, the bony OSL looks white and bright, while the soft-tissue bridge and BM regions look dark. In our initial motion measurements, we presumed that the whole dark region was the BM, and only after we compared the width of this region directly to histological anatomy, did we realize that the dark region included both the bridge and BM. Because of this, during motion measurements, the anatomical boundaries of the OSL, CP bridge and BM were based on (i) the lateral edge of the bony OSL (clearly visible under the microscope used during the experiment), (ii) the edge of the spiral ligament (also visible under the microscope, and

experimentally defined as the most lateral CP place where the velocity was close to the noise floor), and (iii) the width-ratio of the BM and CP bridge (bridge width/BM width = 0.83 ± 0.12 standard deviation, in the cochlear base as measured in histology).

In six histologically-prepared temporal bones stained with Hematoxylin and Eosin from the Otopathology Laboratory at our institution, we estimated the bridge/BM width ratios in the base. In additional 15 specimens we confirmed the presence of the bridge throughout the whole cochlear length. BM width was defined as the width between the basilar crest and the inner-sulcus cell that is adjacent to the bottom of the inner hair cells and close to the habenula perforata (28, 29). Bridge width was the width between the lateral edge of the bony OSL and the BM. These widths were measured from 20 μm, mid-modiolar sectioned slides cut in the vertical plane (2). The locations examined were ∼6 mm from the cochlear base and thus 4–5 mm apical from our motion-measurement location. Sections that are perpendicular to the CP at the motion-measurement location in the cochlear hook require an unusual cutting plane and were not available. However, since there was little difference in the bridge-width/BM-width ratio at other cochlear locations throughout the mid-modiolar sections, we expect that there are no substantial differences in this ratio from the basal anatomical measurement location to the motion-measurement location. The image in Figs. 1B and S1A was chosen as a representative example from the six human temporal bones that we analyzed. The images in Figs. 1A, S1, and S2 were from the basal and apical turns of a guinea pig, mouse, gerbil, cat, and chinchilla cochleas, also from the Otopathology Laboratory collection. Cochleas of at least three different animals from each species were studied and a representative section was chosen for the image of each species.

Calculating Q values. We quantified tuning sharpness by the quality factor, $Q_{10} = f/\Delta f$, where f=BF and Δf is the bandwidth between the frequencies at which the response decreased by 10 dB from the maximum. For our human data, the sparse frequency sampling of 10 points per octave affected the accuracy of measuring both BF and bandwidth. Thus the Q_{10} values are accurate only within ∼15%, based on Q_{10} values of frequencies neighboring the BF and their bandwidths. We calculated Q_{10} values for animal experiments from data extracted from published post mortem (or high-level) tuning curves using "DataThief" software (https://datathief.org/).

References

1. Raufer S, Cho NH, Guinan JJJ, Puria S, Nakajima HH (2019) The Anatomy and Cochlear Partition Motion-Pattern of the Human is Different from those of Laboratory Animals: Optical Coherence Tomography (OCT) Measurements. *Conference Poster, 42nd Annual MidWinter Meeting of the Association for Research in Otolaryngology.*
2. Merchant SN, Nadol J (2010) *Schuknecht's Pathology of the Ear* eds. Merchant SN, Nadol J. (PMPH, USA), 3 edition.
3. Fernández C (1952) Dimensions of the Cochlea (Guinea Pig). *The Journal of the Acoustical Society of America* 24(5):519–523.
4. Ehret G, Frankenreiter M (1977) Quantitative Analysis of Cochlear Structures in the House Mouse in Relation to Mechanisms of Acoustical Information Processing. *Journal of Comparative Physiology* 122:65–85.
5. Plassmann W, Peetz W, Schmidt M (1987) The Cochlea in Gerbilline Rodents. *Brain, Behavior and Evolution* 30:82–101.
6. Cabezudo LM (1978) The Ultrastructure of the Basilar Membrane in the Cat. *Acta Oto-Laryngologica* 86:160–175.
7. Bohne BA, Carr CD (1979) Location of structurally similar areas in chinchilla cochleas of different lengths. *The Journal of Acoustical Society of America* 66:411–414.
8. Greenwood DD (1990) A cochlear frecuency-position function for several species–29 years later. *Journal of the Acoustical Society of America* 87(6):2592–2605.
9. Warren RL, et al. (2016) Minimal basilar membrane motion in low-frequency hearing. *Proceedings of the National Academy of Sciences* 113(30):E4304–E4310.
10. Cooper NP (2000) Radial variation in the vibrations of the cochlear partition in *Recent Developments In Auditory Mechanics*, eds. Wada H, Takasaka T, Ikeda K, Ohyama K. (World Scientific), pp. 109–115.
11. Homer M, Champneys A, Hunt G, Cooper N (2004) Mathematical modeling of the radial profile of basilar membrane vibrations in the inner ear. *The Journal of the Acoustical Society of America* 116(2):1025–1034.
12. Cleveland WS (1993) *Visualizing Data.* (Hobart Press), 1 edition.
13. Corti (1854) Recherches sur l'organe de l'ouïe des mammiferes. *Zeitschrift fuer wissenschaftliche Zoologie* 3(4).
14. Neubert K (1950) Die Basilarmembran des Menschen und ihr Verankerungssystem. *Zeitschrift für Anatomie und Entwicklungsgeschichte* 114:540–590.
15. Fleischer G (1973) Studien am Skelett des Gehoerhörgans der Säugetriere einschließlich des Menschen. *Säugetrierkundliche Mitteilungen* 2(3):131–239.
16. Küçük B, et al. (1991) Microstructures of the Bony Modiolus in the Human Cochlea : A Scanning Electron Microscopic Study. *Journal of Electron Microsc* 40(40):193–197.
17. Shepherd RK, Colreavy MP (2004) Surface Microstructure of the Perilymphatic Space. 130(May 2004):518–523.
18. Kapuria S, Steele CR, Puria S (2017) Unraveling the mystery of hearing in gerbil and other rodents with an arch-beam model of the basilar membrane. *Scientific Reports* 7:228.
19. Taber A, Steele CR (1981) Cochlear model including three-dimensional fluid and four modes of partition flexibility. *Journal of the Acoustical Society of America* 70(2):426–436.
20. Rhode S (1971) Observations of the Vibration of the Basilar Membrane in Squirrel Monkeys using the Mossbauer Technique. *Journal of the Acoustical Society of America* 49(4):1281–1231.

21. Nakajima HH, et al. (2009) Differential Intracochlear Sound Pressure Measurements in Normal Human Temporal Bones. *Journal of the Association for Research in Otolaryngology* 10(1):23–36.
22. Frear D, Guan X, Stieger C, Rosowski JJ, Nakajima HH (2018) Impedances of the inner and middle ear estimated from intracochlear sound pressures in normal human temporal bones. *Hearing Research* 367:17–31.
23. Cooper NP, Rhode WS (1992) Basilar membrane mechanics in the hook region of cat and guinea-pig cochleae: Sharp tuning and nonlinearity in the absence of baseline position shifts. *Hearing Research* 63(1-2):163–190.
24. Dong W, Olson ES (2009) In vivo impedance of the gerbil cochlear partition at auditory frequencies. *Biophysical Journal* 97(5):1233–1243.
25. Olson ES (1999) Direct measurement of intra-cochlear pressure waves. *Nature* 402(6761):526–529.
26. Olson ES (2001) Intracochlear pressure measurements related to cochlear tuning. *Journal of the Acoustical Society of America* 110:349–367.
27. Stieger C, Rosowski JJ, Nakajima HH (2013) Comparison of forward (ear-canal) and reverse (round-window) sound stimulation of the cochlea. *Hearing Research* 301:105–114.
28. Bhatt KA, Liberman MC, Nadol J (2001) Morphometric Analysis of Age-Related Changes in the human basilar membrane. *Ann Otol Rhinol Laryngol* 110:1147–1153.
29. Liu W, et al. (2015) Macromolecular organization and fine structure of the human basilar membrane - RELEVANCE for cochlear implantation. *Cell and tissue research* 360:245–262.